

## Article

# Holistic 1D Electro-Thermal Model Coupled to 3D Thermal Model for Hybrid Passive Cooling System Analysis in Electric Vehicles

Danial Karimi <sup>1,2,\*</sup> , Hamidreza Behi <sup>1,2</sup> , Mohsen Akbarzadeh <sup>1,2</sup>, Joeri Van Mierlo <sup>1,2</sup>  and Maitane Berecibar <sup>1</sup>

<sup>1</sup> Research Group MOBI—Mobility, Logistics, and Automotive Technology Research Centre, Vrije Universiteit Brussel, Pleinlaan 2, 1050 Brussels, Belgium; Hamidreza.Behi@VUB.be (H.B.); mohsen.akbarzadeh.sokkeh@vub.be (M.A.); joeri.van.mierlo@vub.be (J.V.M.); Maitane.Berecibar@vub.be (M.B.)

<sup>2</sup> Flanders Make, 3001 Heverlee, Belgium

\* Correspondence: danial.karimi@vub.be; Tel.: +32-(499)-875895

**Abstract:** Thermal management is the most vital element of electric vehicles (EV) to control the maximum temperature of module/pack for safety reasons. This paper presents a novel passive thermal management system (TMS) composed of a heat sink (HS) and phase change materials (PCM) for lithium-ion capacitor (LiC) technology under the premise that the cell is cycled with a continuous 150 A fast charge/discharge current rate. The experiments are validated against numerical analysis through a computational fluid dynamics (CFD) model. For this purpose, a comprehensive electro-thermal model based on an equivalent circuit model (ECM) is designed. The designed electro-thermal model combines the ECM model with the thermal model since the performance of the LiC cell highly depends on the temperature. Then, the robustness of the model is evaluated using a precise second-order ECM. The extracted parameters of the electro-thermal model are verified by the experimental results in which the voltage and temperature errors are less than  $\pm 5\%$  and  $\pm 4\%$ , respectively. Finally, the thermal performance of the HS-assisted PCM TMS is studied under the fast charge/discharge current rate. The 3D CFD results exhibit that the temperature of the LiC when using the PCM-HS as the cooling system was reduced by 38.3% (34.1 °C) compared to the natural convection case study (55.3 °C).

**Keywords:** electro-thermal model; thermal management system; phase change material; heat sink; electric vehicles



**Citation:** Karimi, D.; Behi, H.; Akbarzadeh, M.; Mierlo, J.V.; Berecibar, M. Holistic 1D Electro-Thermal Model Coupled to 3D Thermal Model for Hybrid Passive Cooling System Analysis in Electric Vehicles. *Energies* **2021**, *14*, 5924. <https://doi.org/10.3390/en14185924>

Academic Editor: Mario Marchesoni

Received: 27 August 2021

Accepted: 15 September 2021

Published: 18 September 2021

**Publisher's Note:** MDPI stays neutral with regard to jurisdictional claims in published maps and institutional affiliations.



**Copyright:** © 2021 by the authors. Licensee MDPI, Basel, Switzerland. This article is an open access article distributed under the terms and conditions of the Creative Commons Attribution (CC BY) license (<https://creativecommons.org/licenses/by/4.0/>).

## 1. Introduction

The main challenge of creating a safe and reliable means of transport that is economical and less pollutant is the energy issue [1]. In such respect, automotive industries are moving from conventional vehicles to electric vehicles (EVs) [2]. The vital part of EVs is the energy storage system (ESS) that is mainly based on lithium-ion batteries (LiBs) due to high energy density [3]. Nevertheless, limited lifetime and low power densities are among their significant drawbacks [4]. On the other hand, supercapacitors (SCs) are high-power ESSs with a very long cycle life but very low energy density [5]. In this context, to overcome the drawbacks of the LiBs and SCs, new hybrid technology has emerged with higher energy density than the SCs, and higher power density than the LiBs, which is called lithium-ion capacitor (LiC) [6]. However, the performance of the LiCs depends highly on temperature [7]. Therefore, a reliable thermal management system (TMS) is essential to guarantee a safe and reliable operation under high current profiles [8]. Such a management system is based on efficient modeling tools, including 1D electro-thermal models and 3D computational fluid dynamics (CFD) models [9].

A validated 1D/3D model is essential for LiCs as they operate in high dynamic current rates. A 1D electro-thermal model for a LiC cell was introduced by Omar et al. [10] that

was the extension model of the Zubieta model for EDLCs. The model had three capacitors and two resistances that could predict the LiC behavior under a constant charge/discharge current rates up to 50 A for different temperature ranges ( $-18\text{ }^{\circ}\text{C}$  to  $+60\text{ }^{\circ}\text{C}$ ). It is clear that the model cannot predict high current rates and does not contain a thermal model. The next article in the literature that developed an electrical model for the LiC cell was published by Firouz et al. [11]. He used a parameter identification system in both time and frequency domain using a wide range of frequency impedance spectroscopy (10 kHz–20 mHz) at various currents, state of charges (SoC), and temperatures ( $-10\text{ }^{\circ}\text{C}$  to  $+60\text{ }^{\circ}\text{C}$ ). The proposed model combined the time and frequency domains to identify the electrical parameters in the functioning of current and SoC. The proposed model has not developed a linked thermal model. The last work in the literature for 1D modeling of the LiCs, to the author's knowledge, was proposed by Soltani et al. [12], in which first and second-order equivalent circuit models (ECM) for high current rates at different temperatures ( $-20\text{ }^{\circ}\text{C}$  to  $+60\text{ }^{\circ}\text{C}$ ). In addition, a thermal model is linked to the electrical model to identify the thermal parameters of the LiC. The accuracy of the proposed electro-thermal model was  $\pm 5\%$ . However, a 3D CFD model was not developed to be linked to the 1D model. Therefore, there is a need for a 1D–3D linked electro-thermal to be validated in real applications for high current rates. There is no more investigation on the 1D electro-thermal modeling for the LiCs in the literature.

On the other hand, a 3D model can simulate the cell's behavior at high current rates where the temperature of the cell goes beyond the safe limit ( $+40\text{ }^{\circ}\text{C}$ ) and requires a robust cooling system [13]. Cooling techniques for ESSs are divided into two methods, including active and passive methods [14,15]. The active method comprises the air cooling technique [16] and the liquid cooling technique [17]. These two active methods have high cooling capabilities [18], but they require an external power source to operate, and their maintenance costs are also high due to moving parts [19]. The passive method comprises heat pipes [20], heat sinks [21], and phase change materials (PCM) [22,23]. Heat pipes are passive high thermal conductive systems that should be used as secondary condensers [24,25]. In addition, heat pipes are gravity-dependent with complex designs [26]. Heat sinks increase the heat flow away from a heat source by increasing the device's surface area. Heat sinks are not good solutions for high power applications when using as a first cooling system, but in the case of using as a secondary cooling system, they show high performance. PCM is another passive system, which absorbs large amounts of latent heat through a phase change transition [27]. However, PCMs cannot release all the absorbed heat since they have very low thermal conductivity [28]. Therefore, an added material should be added to the PCMs to increase the thermal conductivity and help reject the absorbed heat to the ambient. The secondary material that can be added to the PCM would be aluminum mesh grid [29], copper mesh grid [30], nano-particles [31], heat pipes [32], heat sinks [33], or even active systems like liquid [34] or a fan [35].

A 1D electrical model is developed at the first stage of the present work, and the electrical parameters of the LiC cell are extracted. Then, a 1D thermal model is developed linked to the electrical model to make a robust 1D electro-thermal platform capable of identifying the electro-thermal parameters. The characterization tests have been carried out within a wide range of temperatures from  $-30\text{ }^{\circ}\text{C}$  to  $+60\text{ }^{\circ}\text{C}$ . Such a very cold temperature has never been carried out before showing the uniqueness of the present work. In addition, the current rates applied to the cell are pretty high, from 0.1 A to 500 A, which shows the work's uniqueness in the field of electro-thermal modeling. Later, the extracted parameters will be the input to the 3D thermal model to be validated against the experiments. This work aims at proposing a hybrid TMS employing PCM and a novel lightweight heat sink (PCM-HS) to control the temperature of the LiC under high current rates. The hybrid PCM-HS TMS is validated through a robust 3D CFD simulation platform linked to the developed 1D electro-thermal model. To the authors' best knowledge, such a comprehensive 1D–3D tool is not addressed in the literature.

The structure of the paper is as follows: Section 2 deals with the chemistry and characterization of the LiC cell. Section 3 presents the hybrid TMS based on PCM and heat sink. The 3D CFD thermal model is introduced and validated in Section 4. Furthermore, in Section 5, results and discussion are given. The last section provides the conclusion and critical features of this work.

## 2. Chemistry and Characterization of the LiC

### 2.1. LiC 2300 F Technology

In this study, the target cell is a commercial prismatic LiC cell with 2300 F capacitance. The LiC is a hybrid technology that is categorized between LiBs and EDLCs that has no symmetric structure. The cathode of the LiC is made of porous activated carbon (AC), and the anode is made of carbon with doped li-ion. In addition, Lithium salt is used as an electrolyte. The LiC can be cycled with current rates of up to 300 A for continuous currents and 500 A for pulse currents. Therefore, in this work, a high duty current rate is applied to the cell to extract the cell's electrical and thermal parameters, which will then be used for the 3D CFD simulation studies. The characteristics of the target LiC cell are shown in Table 1. In addition, the schematic of the cell with all the dimensions is depicted in Figure 1.

**Table 1.** Specifications of the 2300 F LiC cell.

Parameters	Value	Unit
Rated Capacitance	2300	F
Voltage Range	2.2 to 3.8	V
Nominal Voltage	3	V
Weight	0.355	kg
Working Temperature	−30 to +70	°C

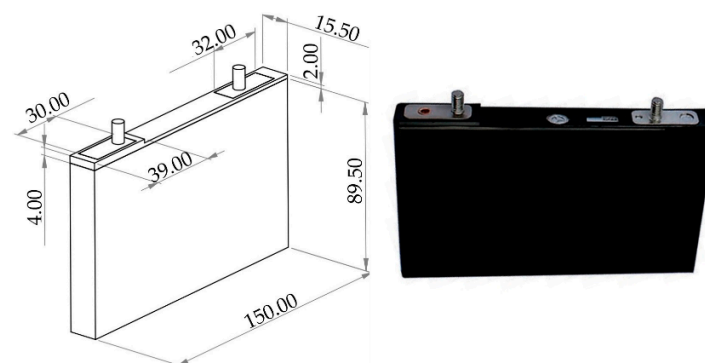


**Figure 1.** The dimensions and layout of the lithium-ion capacitor cell.

### 2.2. Characterization Test Protocol

The facilities of the MOBI laboratory in the ETEC department of the Vrije Universiteit Brussel were employed for the experimental tests. In this context, PEC battery tester and cycler were used to characterize and cycle the LiC cell. A climate chamber was employed to keep the temperature at a controlled test condition. K-type thermocouples and a data logger were linked to a computer in each time step to measure the temperature. The test protocol is demonstrated in Figure 2, showing all the tests needed to characterize the cell and extract the electrical and thermal parameters of the LiC. The characterization tests have been carried out within a wide range of temperatures from  $-30\text{ }^{\circ}\text{C}$  to  $60\text{ }^{\circ}\text{C}$ . In addition, the current rates applied to the cell are pretty high, from 0.1 A to 500 A, which shows the work's uniqueness in the field of electro-thermal modeling.

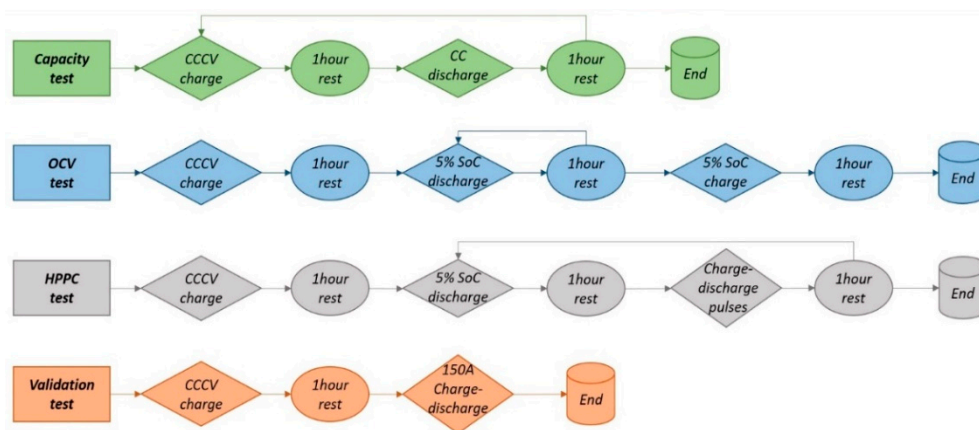


**Figure 2.** The test protocol of the characterization tests.

### 2.2.1. Electrical Characterization

The electrical characterization is the first essential step to identify the LiC cell parameters. Therefore, some tests should be carried out to characterize the cell under some predefined conditions. The electro-thermal tests are conducted employing the battery cyclers and the climate chamber. The experimental process consists of a pre-conditioning test, capacity test, open-circuit voltage (OCV) test, hybrid pulse power characterization (HPPC) test, and validation test.

The first test is a pre-conditioning test that includes ten cycles of 10C (C refers to the rated capacitance) constant-current, constant-voltage charge (CCCV), and constant-current (CC) discharge. Each of the ten cycles consists of ten minutes rest in the end to activate the ion kinetics. After the pre-conditioning test, the capacity of the cell should be checked using a capacity test. This test includes a 1C CCCV charge and CC discharge with 30 min rest in between.

The most crucial test to characterize the state of charge (SoC) of the LiC cell is the OCV test, which is a standardized test. In the OCV test, the cell is fully charged with a 1C CCCV step. The cell rests for an hour, and then a 5% SoC discharge procedure is carried out to reach the lower voltage limit of the cell. After every discharge procedure, one hour of rest should be imposed to stabilize the OCV test. The next step of the OCV test is to charge the cell with 5% CC fully.

The pulse power capability of the LiC cell is studied by the HPPC test conducted at different SoC. First, the cell is fully charged with a 1C CCCV procedure before an hour rest period. The cell is then discharged by 5% with a 1C-rate. After a similar rest period, a set of 20 A, 100 A, and 200 A charge and discharge pulses complement the Ah change in the cell. This process is continued until the cell reaches the cut-off voltage limit. Figure 2 exhibits the test protocol for the 150 A charge/discharge current rate.

### 2.2.2. Thermal Characterization

The thermal characterization test includes single charge/discharge current pulses ranging from 50 A to 500 A and continuous currents from 50 A to 300 A. The data logger linked to a computer is responsible for monitoring the temperature at every time step using the K-type thermocouples. The mentioned current rates are applied to the LiC while the cell is cycled between its lower and upper cut-off voltages from 2.2 V to 3.8 V until the cell is in thermal equilibrium with the chamber's temperature.

### 2.3. Governing Equations of the Electro-Thermal Model

The electro-thermal model of the LiC cell has been developed in this section for a wide temperature range from  $-30\text{ }^{\circ}\text{C}$  to  $+60\text{ }^{\circ}\text{C}$ . The LiC technology is emerged to operate in high power applications where high peak current rates are required. In this regard,

the electrical and thermal models are explained below that will be implemented in the MATLAB environment for 1D simulations.

### 2.3.1. Electrical Model

A second-order equivalent circuit model (ECM) including an ohmic resistance ( $R_0$  [ $\Omega$ ]) representing the resistance of the charge transfer in the electrolyte side, two RC branches representing the polarization of the electrode and contact resistance between the domains of electrode and electrolyte ( $R$  for polarization resistance ( $R_p$  [ $\Omega$ ]) and  $C$  for capacitance ( $C_p$  [F])), and a voltage source [36]. These parameters depend highly on the current rates, operating temperature, and state of charge (SoC). The terminal voltage ( $V_t$  [V]) is then expressed as:

$$V_t = OCV(SoC, T) - I_L R_0(SoC, T, I_L) - V_{CP1}(SoC, T, I_L) - V_{CP2}(SoC, T, I_L) \quad (1)$$

$$\frac{dV_{CPi}}{dt} = -\frac{1}{R_{Pi}C_{Pi}}V_{CPi} + \frac{1}{C_{Pi}}I_L \quad (2)$$

$$\tau_i = R_{Pi}C_{Pi} \quad (3)$$

The OCV [V] represents the open-circuit voltage of the cell. In addition,  $I$  [A] denotes the current of the cell. The  $CP1$  and  $RP1$  are for the first RC branch, while  $CP_2$  and  $RP_2$  are for the second RC branch. The estimated parameters in the developed model are stored in look-up tables (LUTs).

### 2.3.2. Thermal Model

The thermal model is an essential part of the 1D model development since the electrical parameters depend highly on temperature. The relationship between electrical and thermal parameters is shown in Figure 3. The generated heat of the cell is then measured in this section through the thermal model. The heat source, the ambient temperature, and the initial temperature are among the parameters that are input to the model. The heat is generated during the charge or discharge processes due to reversible heat (entropy change) and irreversible heat (internal resistance) [37]. The total generated heat of the cell ( $P_{loss}$  [W]) can be expressed as follows:

$$P_{loss} = I_L^2 R_0(SoC, T, I_L) + I_{RP1}^2 R_{P1}(SoC, T, I_L) + I_{RP2}^2 R_{P2}(SoC, T, I_L) - I_L T_{cell} \frac{\partial OCV(T_{cell}, SoC)}{\partial T_{cell}} \quad (4)$$

where  $C_{th}$  [J/K],  $R_{th}$  [K/W], and  $R_{con}$  [K/W] denote the thermal capacity, thermal conductive resistance, and thermal convective resistance.

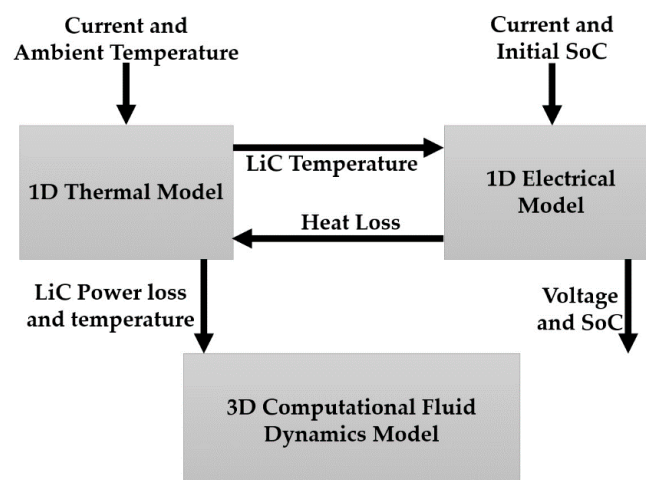


Figure 3. The connection between electrical and thermal models.

For the proposed thermal circuit, the surface temperature ( $T_s$  [K]) is calculated [38]:

$$T_s(t) = \left( 1 - e^{\frac{-\Delta t}{C_{th}(R_{th} + R_{con})}} \right) (P_{loss}(t)R_{con} + T_a) + T_s(t - \Delta t)e^{\frac{-\Delta t}{C_{th}(R_{th} + R_{con})}} \quad (5)$$

where  $P_{loss}$  [W],  $T_{int}$  [K],  $T_{cell}$  [°C],  $T_a$  [K], and  $T_s$  denote the cell's power loss, internal temperature, the cell's temperature, ambient temperature, and the cell's surface temperature.

### 3. Hybrid TMS Development

A robust hybrid TMS using phase change materials (PCM) and heat sink (HS) is proposed in this section to cool down the LiC cell. Then, the experimental results are validated against the 3D CFD model developed based on the 1D electro-thermal model in the previous section.

#### 3.1. Experimental Test Bench

The experimental test bench for the proposed TMS is composed of the LiC 2300 F prismatic cell, paraffin PCM, two aluminum heat sinks, a data logger, K-type thermocouple, a battery cycler, a climate chamber, and a computer. The test bench facilities are demonstrated in Figure 4. The PCM and HS properties are listed in Table 2.

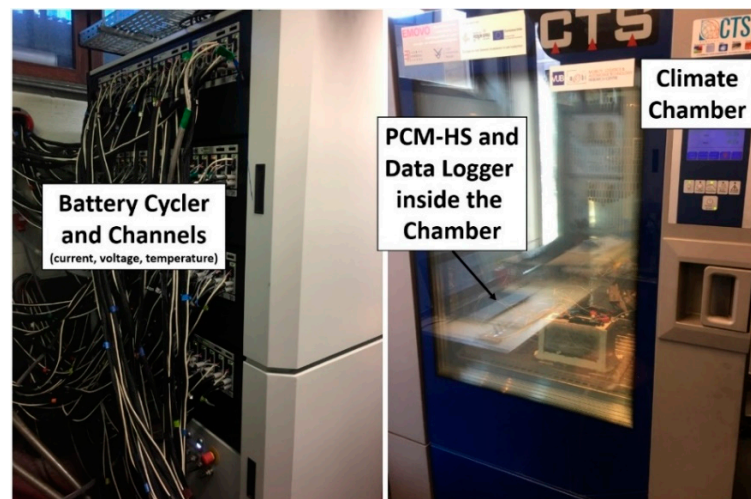


**Figure 4.** Test bench facilities, including the battery cycler with 80 channels, a climate chamber, a data logger with thermocouples, and the PCM-HS inside the chamber.

**Table 2.** The PCM and HS properties.

	Parameter	Value	Unit
PCM	Material	Paraffin	/
	Latent heat of fusion	236	kJ/kg
	Melting temperature	32–44	°C
	Thermal conductivity	0.2	W/m·K
HS	Material	Aluminum	/
	Dimension	77 × 40 × 7	mm
	Density	2700	Kg/m <sup>3</sup>
	Specific heat	963	J/kg·K
	Thermal conductivity	218	W/m·K

The error of the test bench facilities is utilized to calculate the uncertainty analysis. Based on the Schultz and Cole method, the error of uncertainty for the experiments can be expressed as follows [39]:

$$U_R = \left[ \sum_{i=1}^n \left( \frac{\partial R}{\partial V_I} U_{V_I} \right)^2 \right]^{1/2} \quad (6)$$

where  $U_{V_I}$  represents the error of every single factor and  $U_R$  shows the total errors. The maximum uncertainty of our test bench for the 1D electro-thermal tests and the 3D CFD test is around 2.01%.

### 3.2. Experimental Results

In this section, the monitored temperature by the data logger linked to a computer is explained. Four different case studies have been investigated, including thermal behavior of the LiC under the natural convection (NC), thermal behavior of the LiC when pure PCM is used as a passive cooling system, and thermal behavior of the cell when a hybrid TMS is employed to cool down the LiC.

#### 3.2.1. NC

The cell is put inside the climate chamber when the fan is off to avoid increasing the convective heat transfer coefficient. Therefore, this section aims to investigate the cell's temperature under NC, not forced convection. The high current rate of 150 A is applied to the cell continues to cycle the LiC at high current rates. Such a high current rate can be defined as high power applications in electric vehicles for acceleration or when high peak power is required for traction.

The experimental results show that the LiC's temperature exceeds the safe limit and proves that a robust TMS is mandatory for such a high-power application. The LiC temperature reaches 55.3 °C after 1400 s, which is way beyond the temperature range announced by the manufacturer. Figure 5 shows the temperature curve of the LiC under the NC case study.

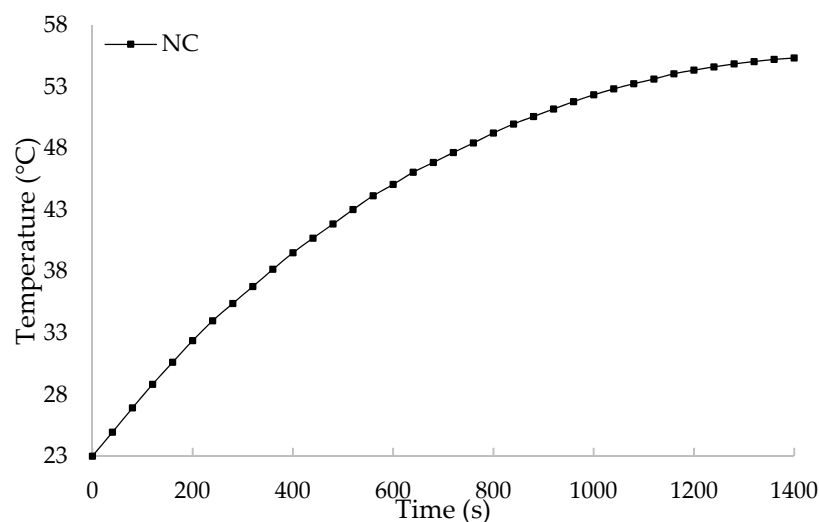


Figure 5. Experimental results for the LiC cell under NC case study.

#### 3.2.2. PCM

In the next step of the experimental tests, the pure paraffin PCM is poured into the polyvinyl chloride (PVC) container around the cell to absorb the cell's heat. The maximum temperature of the cell is 40.8 °C that is almost close to the safety setpoint for 150 A current rate. However, it should be enhanced due to the LiC applications up to 300 A. As is evident, PCM can absorb the generated heat of the LiC during the cycling thanks to its high latent heat of fusion. However, the pure PCM cannot release the absorbed heat to the ambient

due to its very low thermal conductivity of around  $0.2 \text{ W/m}\cdot\text{K}$ . Therefore, a secondary cooling system is needed to be added to the PCM TMS to increase its ability to remove the heat. Figure 6 illustrates the temperature evolution of the LiC when using the PCM as the cooling system.

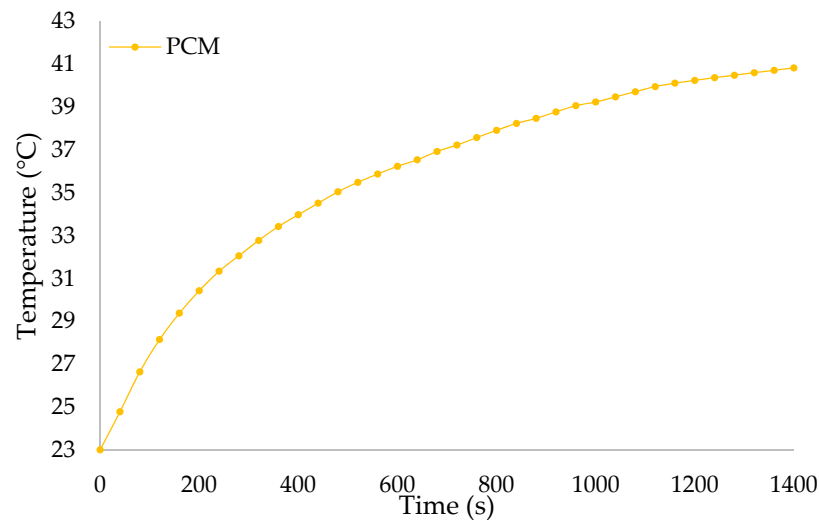


Figure 6. Experimental result for the LiC cell employing PCM TMS case study.

Compared to the NC case study, pure PCM reduces the temperature by 26.2%, perfect for a system that does not require any external power source to operate. Therefore, such a passive system can be used for thermal storage or as a hybrid system to control the temperature of the LiC in high-power applications for electric vehicles.

### 3.2.3. Hybrid PCM-HS

In this section, the low thermal conductivity of the PCM is compensated using two heat sinks on both sides of the cell. Hence, a hybrid TMS is proposed that is also called HS-assisted PCM TMS. The results of the proposed hybrid TMS are demonstrated in Figure 7. As shown, the maximum temperature of the cell after 1400 s intense high current charging/discharging with a 150 A current rate is around  $38.3 \text{ }^\circ\text{C}$ , which is quite good in controlling the maximum temperature at the desired range.

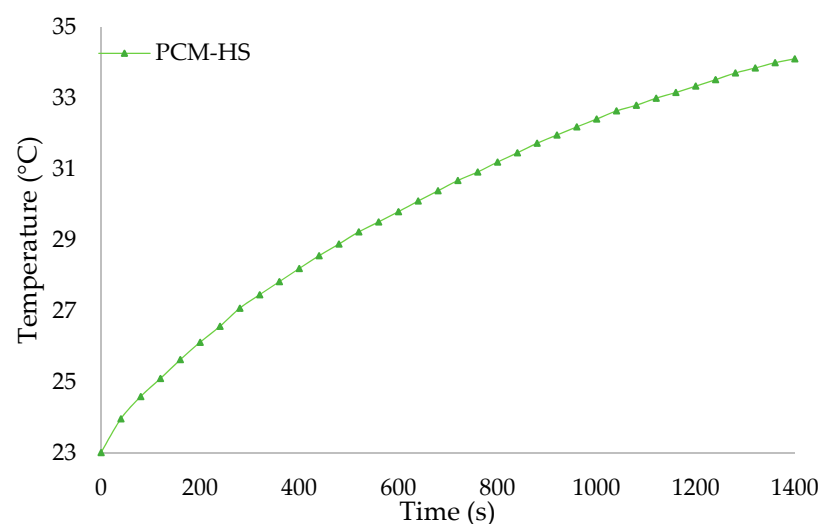


Figure 7. Experimental results for the LiC cell employing hybrid PCM-HS case study.

The hybrid PCM-HS reduces the maximum temperature by 38.3% compared to the NC case study and 16.4% to the pure PCM cooling system. Therefore, such a hybrid system has the high thermal performance to be used in high power applications.

### 3.2.4. Comparison of the Results

The experimental results for three use cases, including NC, PCM, and PCM-HS case studies, are explained in this section to have the insight to compare the results regarding which system has better performance. In such respect, the results are depicted in Figure 8 and compared in Table 3.

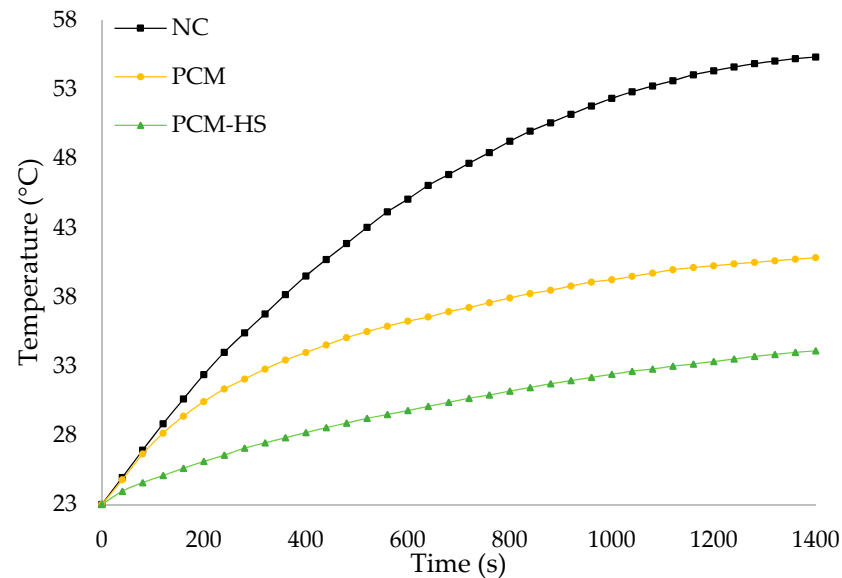


Figure 8. Comparison of the experiments for NC, pure PCM, and hybrid PCM-HS.

Table 3. Comparison of the experimental results for three case studies.

	NC	PCM	Hybrid PCM-HS
Max. Temperature (°C)	55.3	40.8	34.1
Temperature reduction	-	26.2%	38.3%
Difference with ambient (°C)	32.3	17.8	11.1

## 4. CFD Model Development

The output of the 1D electro-thermal model used for the 3D model development is the LiC temperature and power loss. The 1D model's output is linked to the CFD model in this section to make a 1D–3D robust model capable of extracting the electrical and thermal parameters and simulating the CFD model.

### 4.1. Model Development and Equations

#### 4.1.1. 3D Heat Generation

The energy equation for the 3D thermal model that is developed through the finite element method (FEM) is described as follows:

$$\rho C_p \frac{dT}{dt} = \left[ \lambda_x \frac{\partial^2 T}{\partial x^2} + \lambda_y \frac{\partial^2 T}{\partial y^2} + \lambda_z \frac{\partial^2 T}{\partial z^2} \right] + P_{loss} \quad (7)$$

where  $\rho$  [kg/m<sup>3</sup>] denotes the density,  $C_p$  [J/kg·K] is the heat capacity,  $T$  [K] is the temperature,  $\lambda$  [W/m·K] represents thermal conductivity, and  $P_{loss}$  [W/m<sup>3</sup>] represents the volumetric heat generation.

As mentioned in the electrical modeling section, the LiC's heat generation comprises two heat sources, including reversible and irreversible [40]:

$$P_{loss} = I (OCV - V_t) - I T \frac{\partial U}{\partial T} \quad (8)$$

$$P_{loss} = \frac{R I^2}{V_{tab}} \quad (9)$$

$$R = \rho' \frac{l}{S} \quad (10)$$

where  $V_{tab}$  [V] is the tab volume,  $\rho'$  [ $\Omega\text{m}$ ] denotes the resistivity,  $l$  [m] is the length, and  $S$  [ $\text{m}^2$ ] represents the cross-sectional area. The heat is generated during the charge/discharge cycle tests, where 150 A flows through the positive (cathode) and negative (anode) tabs. The positive tab is made of aluminum, and the negative tab is made of copper. The physical parameters of the cell utilized in the 3D CFD simulation studies are listed in Table 4 [19].

**Table 4.** Physical parameters of the LiC used in the 3D CFD model [19].

Parameter	Electrode Domain	Positive Tab	Negative Tab	Units
Density	1500	2700	8960	$\text{Kg}/\text{m}^3$
Thermal conductivity	$\lambda_{layer} = 5; \lambda_{planar} = 0.3;$	238	400	$\text{W}/\text{m}\cdot\text{K}$
Specific heat	641	900	385	$\text{J}/\text{kg}\cdot\text{K}$

#### 4.1.2. Heat Sink (HS) Modeling

The heat transfer rate associated with the HS is modeled in this section. The first step to model the HS numerically is knowing the temperature profile. Some assumptions should be made to simplify the model and reduce the computational cost. In this regard, due to the small dimensions of the HS, the conduction is assumed to take place only in the longitudinal ( $x$ -) direction, even if conduction within the HS is two-dimensional. The dimensions of the used HS are shown in Figure 9. Moreover, the temperature change in the transverse directions ( $y$ -,  $z$ -) are small. Hence, the thermal conductivity ( $K$  [ $\text{W}/\text{m}\cdot\text{K}$ ]) is assumed constant, and the surface radiation is negligible. The other assumption is related to the convective heat transfer coefficient ( $h$  [ $\text{W}/\text{m}^2\cdot\text{K}$ ]) uniform over the surface. Figure 10 shows the energy balance within the HS that can be expressed as:

$$dq_{conv} = q_x - q_{x+dx} \quad (11)$$

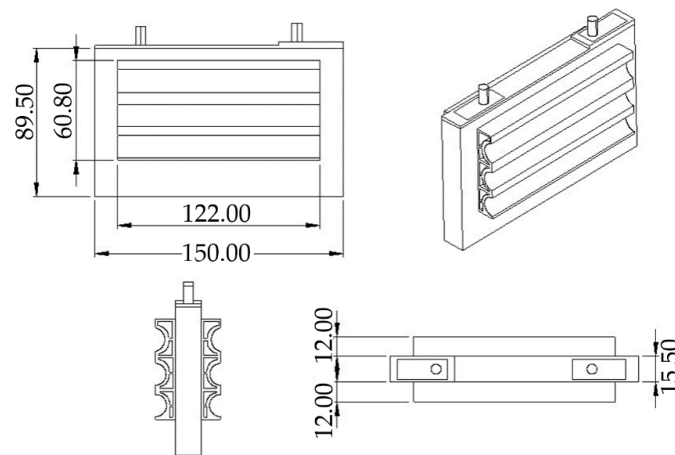


**Figure 9.** The HS dimensions regarding the target LiC cell.

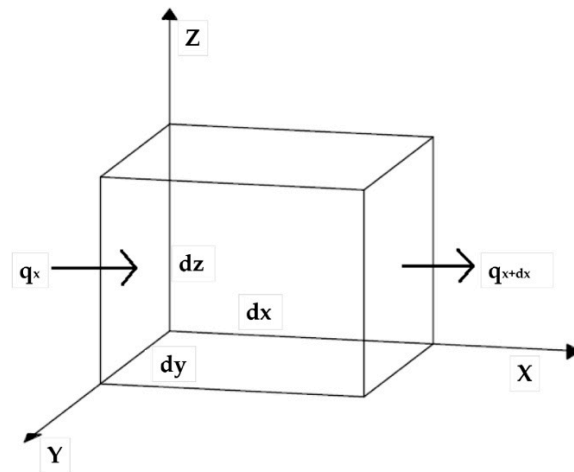


Figure 10. Energy balance within the HS.

Equation (11) expresses that the heat flow is set up from the hot spot to the cold spot. The temperature gradient is inversely proportional to the heat flow, thanks to Fourier's law:

$$q_x = -kA_c \frac{dT}{dx} \quad (12)$$

$$q_{x+dx} = q_x + \frac{dq_x}{dx} dx \quad (13)$$

$$q_{x+dx} = -kA_c \frac{dT}{dx} - k \frac{d}{dx} \left( A_c \frac{dT}{dx} \right) dx \quad (14)$$

where  $A_c$  denotes the cross-sectional area that may vary along the  $x$ -direction. Nevertheless, due to the assumptions, the cross-sectional area is constant:

$$dq_{conv} = h dA_s (T - T_\infty) \quad (15)$$

where  $T_\infty$  is the temperature far from the HS, i.e., ambient temperature. In addition,  $A_s$  is the surface area that can be calculated as:

$$A_s = Px \quad (16)$$

The surface area is measured from  $x$ , the base. In addition,  $P$  is the HS perimeter. By the mentioned equations, the energy equation can be substituted to:

$$\frac{d}{dx} \left( A_c \frac{dT}{dx} \right) - \frac{h}{k} \frac{dA_s}{dx} (T - T_\infty) = 0 \quad (17)$$

The second-order ordinary differential equation (ODE) is given by:

$$\frac{d^2 T}{dx^2} - \frac{hP}{kA_c} (T - T_\infty) = 0 \quad (18)$$

By giving a dimensionless form at Equation (18) by defining two normalized variables:

$$\Theta(x) = (T - T_\infty) \quad (19)$$

$$X = \frac{x}{L} \quad (20)$$

where  $\Theta$  denotes the excess of temperature. By defining a coefficient determining how fast the warm-up fades along with the HS:

$$\lambda^2 = \frac{hPL^2}{kA_c} \quad (21)$$

A linear, homogeneous, second-order differential equation with constant coefficients is achieved:

$$\frac{d^2\Theta}{dX^2} - \lambda^2\Theta = 0 \quad (22)$$

The general solution is given by:

$$\Theta = C_1e^{(\lambda.X)} + C_2e^{(-\lambda.X)} \quad (23)$$

In order to solve Equation (23), we need appropriate boundary conditions. Two cases can be considered:

- (1) The temperature at the base of the HS is fixed, meaning that  $T(x = 0) = T_{battery}$ . Therefore:

$$\Theta(0) = T_{battery} - T_\infty = \Theta_{battery} \quad (24)$$

- (2) The second case occurs at the HS tip ( $x = L$ ) that may correspond to one of the three different physical conditions:

- Conditions 1:  $L \rightarrow \infty$  meaning that the temperature is not too high and the PCM around the HS has not yet melted. The solution becomes:

$$\Theta = e^{(\lambda.X)} \quad (25)$$

- Condition 2: Assuming that the heat dissipation at the tip of the fin is negligible, the adiabatic condition can be assumed ( $\nabla\Theta = 0$  at  $X = 1$ ). The solution is:

$$\Theta = \frac{\cosh(\lambda(1 - X))}{\cosh(\lambda)} \quad (26)$$

- Condition 3: When the side surface does not dissipate all the heat loss of the cell, the tip of the HS is crossed by a convective flux governed by Newton's law:

$$-k \frac{dT}{dx} \Big|_{x=L} = h(T(L) - T_\infty) \quad (27)$$

That can be resumed as:

$$\frac{d\Theta}{dX} = Bi.\Theta \quad (28)$$

where  $Bi$  is the Biot number that quantifies the ratio between the heat evacuated by convection and the heat transmitted by conduction to the solid. The final solution for the HS modeling is:

$$\Theta = \frac{\cosh(\lambda(1 - X)) + \frac{Bi}{\lambda} \sinh(\lambda(1 - X))}{\cosh(\lambda) + \frac{Bi}{\lambda} \sinh(\lambda)} \quad (29)$$

#### 4.1.3. PCM Modeling

The effective heat capacity (EHC) method is employed in this section to model the PCM. Using such a method is the phase transition of the PCM that occurs in a wide temperature range. The adjustment of the enthalpy is also considered in the PCM modeling [41]. The phase transition region (mushy zone) has an essential factor that is called the EHC value. This value is maximum at the mushy zone. The density and thermal conductivity of

the solid and liquid phases are different. Therefore, the average of these two phases should be considered [42]. The EHC ( $C_{peff}$  [J/kg·K]) can be expressed as follows:

$$\rho C_{peff} \frac{\partial T}{\partial t} = \lambda \nabla^2 T \quad (30)$$

$$C_{peff} = \begin{cases} C_{Ps} & T \leq T_s \\ C_{Ps} + a(T - T_s) & T_s < T < T_m \\ C_{Pm} + b(T - T_m) & T_m < T < T_l \\ C_{Pl} & T \geq T_l \end{cases} \quad (31)$$

where indices  $s$ ,  $m$ , and  $l$  represent the solid, mushy, and liquid zones. In addition,  $a$  and  $b$  can be defined as follows:

$$a = \frac{C_{Pm} - C_{Ps}}{T_m - T_s} \quad (32)$$

$$b = \frac{C_{Pl} - C_{Pm}}{T_l - T_m} \quad (33)$$

By knowing the PCM's latent heat of fusion  $dH$  [kJ/kg], the heat capacity in the mushy zone ( $C_{Pm}$  [J/kg·K]) can be calculated:

$$C_{Pm} = \frac{2dH + 2(C_{Pl} - C_{Ps})(T_l - T_m) + C_{Ps}(T_m - T_s) + C_{Pl}(T_l - T_m)}{T_l - T_s} \quad (34)$$

In addition, the effective thermal conductivity ( $k_{eff}$  [W/m·K]) and the effective density ( $\rho_{eff}$  [kg/m<sup>3</sup>]) can be expressed as follows:

$$k_{eff} = \begin{cases} k_s & T \leq T_s \\ \frac{k_s + k_l}{2} & T_s < T < T_l \\ k_l & T \geq T_l \end{cases} \quad (35)$$

$$\rho_{eff} = \begin{cases} \rho_s & T \leq T_s \\ \frac{\rho_s + \rho_l}{2} & T_s < T < T_l \\ \rho_l & T \geq T_l \end{cases} \quad (36)$$

#### 4.2. Boundary Conditions

The boundary condition for all of the surfaces of the system can be defined as the convective heat transfer coefficient ( $h$  [W/m<sup>2</sup>·K]) between the ambient ( $T_\infty$  [°C]) and surface ( $T$  [°C]):

$$-k \frac{\partial T}{\partial n} = h(T - T_\infty) \quad (37)$$

As mentioned earlier,  $k$  is the thermal conductivity. In addition,  $\frac{\partial T}{\partial n}$  denotes the temperature gradient. At the beginning of the numerical computations ( $t = 0$ ), the initial condition of  $T(x, y, z) = T_\infty$  is assumed. Hence, the initial and the ambient temperature of 23 °C is set in the CFD simulation studies. The simulation time for the 3D CFD simulation studies is 1400 s with 1 s step time. The mass of the PCM for the pure PCM case study is 330 g, where the thickness of the PCM around the LiC cell inside the PVC container is 13 mm. The radiation is omitted in the CFD analysis [43].

## 5. Results and Discussion

### 5.1. Results of the 1D Electrical Model

The developed semi-empirical 1D model was modeled in which the OCV model was based on a numerical method that the results are saved in LUTs. Figure 11 demonstrates the OCV map as function of SoC (between 0% to 100%) and temperature (−30, −10, 0, 10, 25, 40, 50, and 60 °C). The ohmic resistance values that were calculated utilizing the least-square fitting method are shown in Figure 12. The ohmic resistance map is a function

of SoC (between 0% to 100%) and temperature ( $-30$ ,  $-10$ ,  $0$ ,  $10$ ,  $25$ ,  $40$ ,  $50$ , and  $60$  °C) for the current rate of  $150$  A that is very high. The extracted parameters are stored in LUTs that are used to calculate the terminal voltage of the LiC.

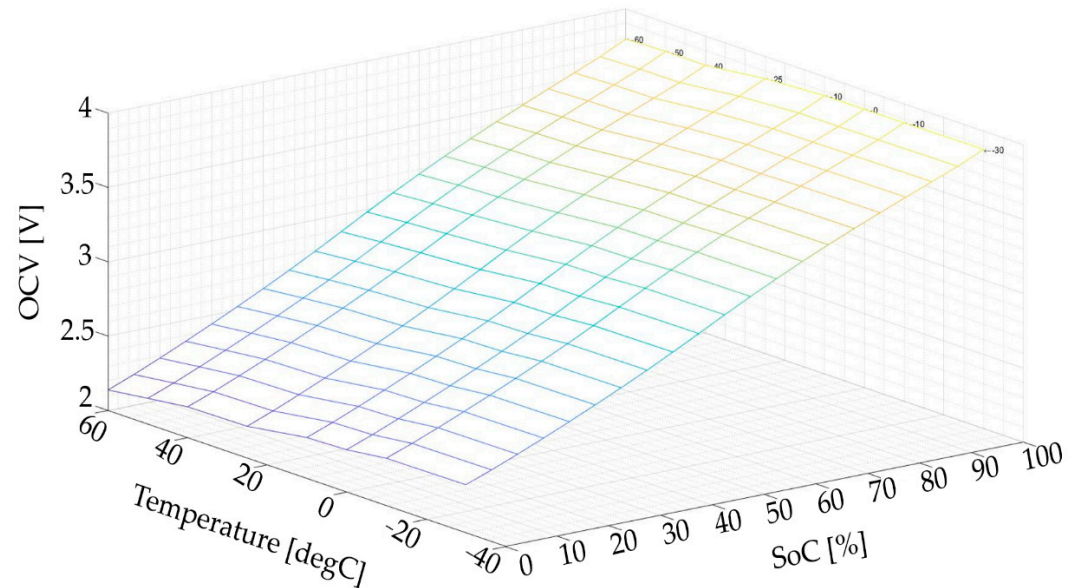


**Figure 11.** The OCV discharge map as a function of SoC and temperature.

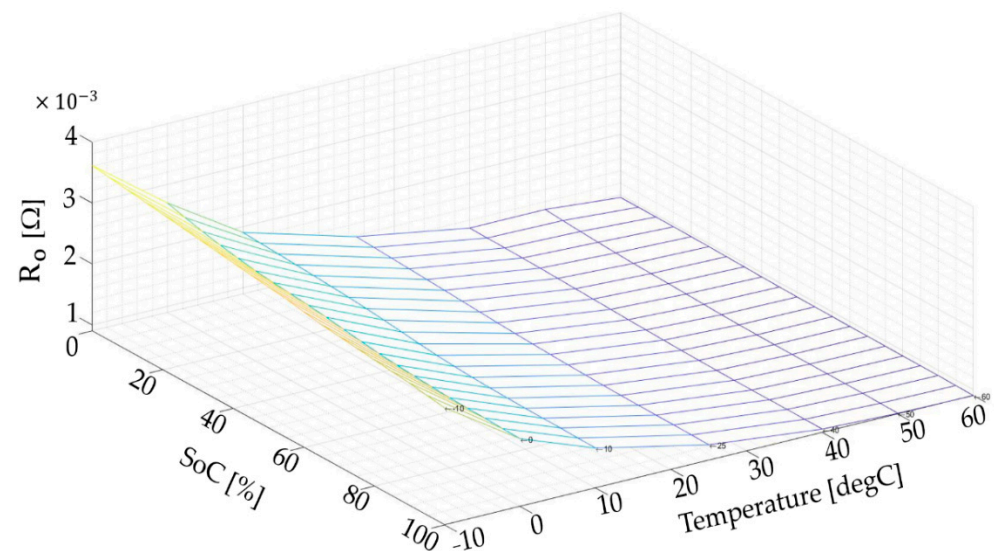


**Figure 12.** The ohmic resistance map as a function of SoC and temperature.

The accuracy of the extracted parameters in the developed 1D model is evaluated in a dynamic driving cycle to be verified against the experimental results. Figure 13a shows a part of the driving cycle consisting of different current rates up to  $300$  A for  $500$  s. The results are compared for voltage in the electrical model and temperature in the thermal model. The experimental and simulation results for voltage are shown in Figure 13b with very low simulation error (Figure 13c). In such a high dynamic current rate that can be used for high power applications, the error for high current rates above  $100$  A is around  $\pm 5\%$  that is very low. For the currents lower than  $100$  A, the simulation error for voltage is remarkably lower than this ( $\leq \pm 3\%$ ), proving the precision of the developed electrical model.

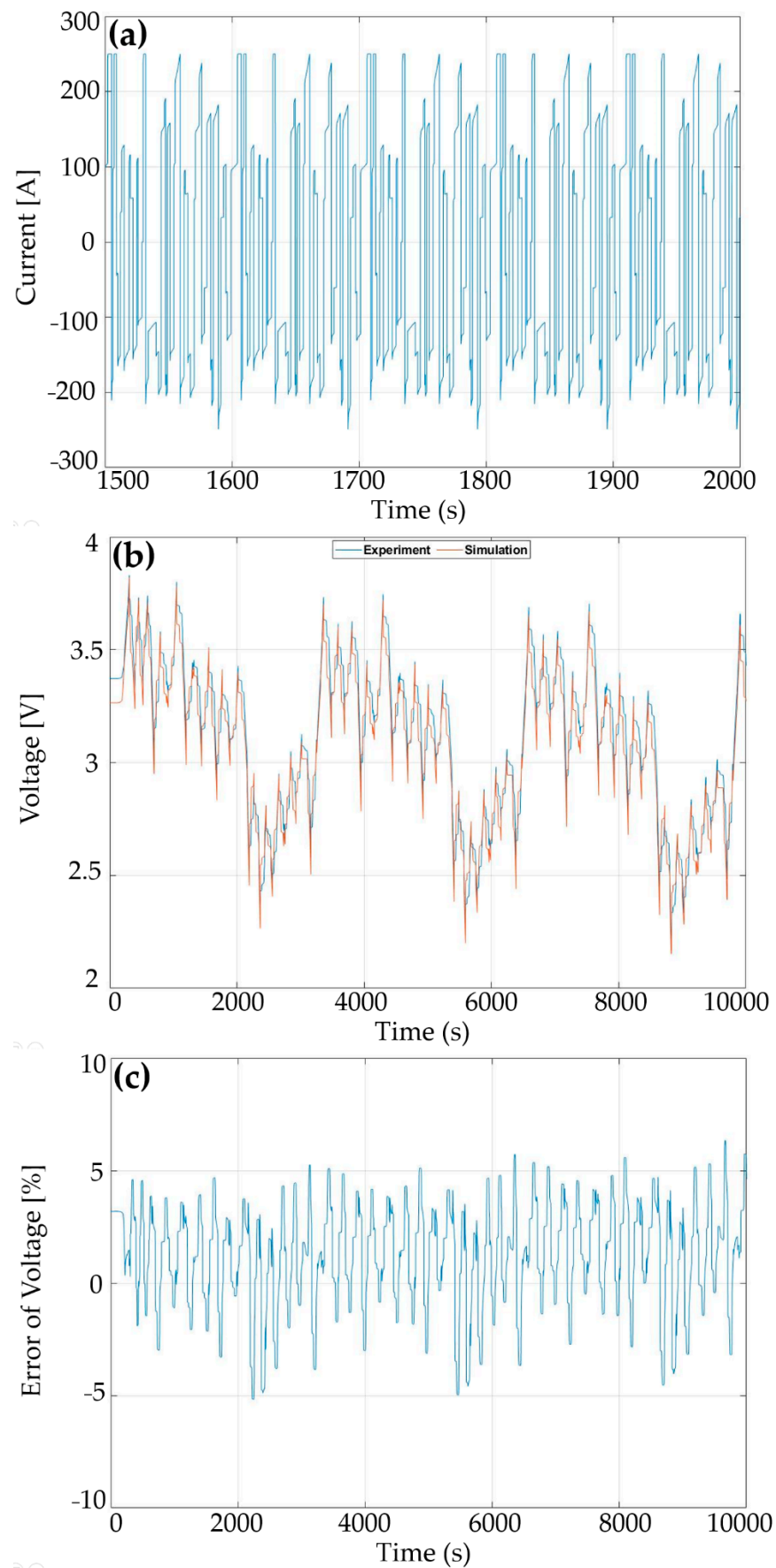


**Figure 13.** The developed 1D electrical model validation with dynamic driving cycle for (a) current rates; (b) experimental and simulation voltage; (c) error of voltage.

### 5.2. Results of the 1D Thermal Model

The temperature error is essential to be as low as possible to simulate the temperature curve highly and to show the precision of the thermal model. In this regard, the temperature curve for the dynamic driving cycle is presented in Figure 14. The temperature of the climate chamber is set at various ranges to perform the experimental thermal test. Therefore, the condition should be considered the forced-flow or forced convection since a fan inside the climate chamber is responsible for controlling the temperature. In the figure, the simulation and experimental results for the temperature with an initial temperature of 24.6 °C as well as the error of temperature are exhibited. As can be seen, the error of temperature in the worst scenario (the highest current rate) is around  $\pm 4\%$ , which shows the very high precision of the thermal model at the beginning of the simulation. After  $5 \times 10^4$  s, where the cell's temperature is at the steady-state zone, the error ranges below  $\pm 2\%$ , which is perfect for such a high dynamic profile.

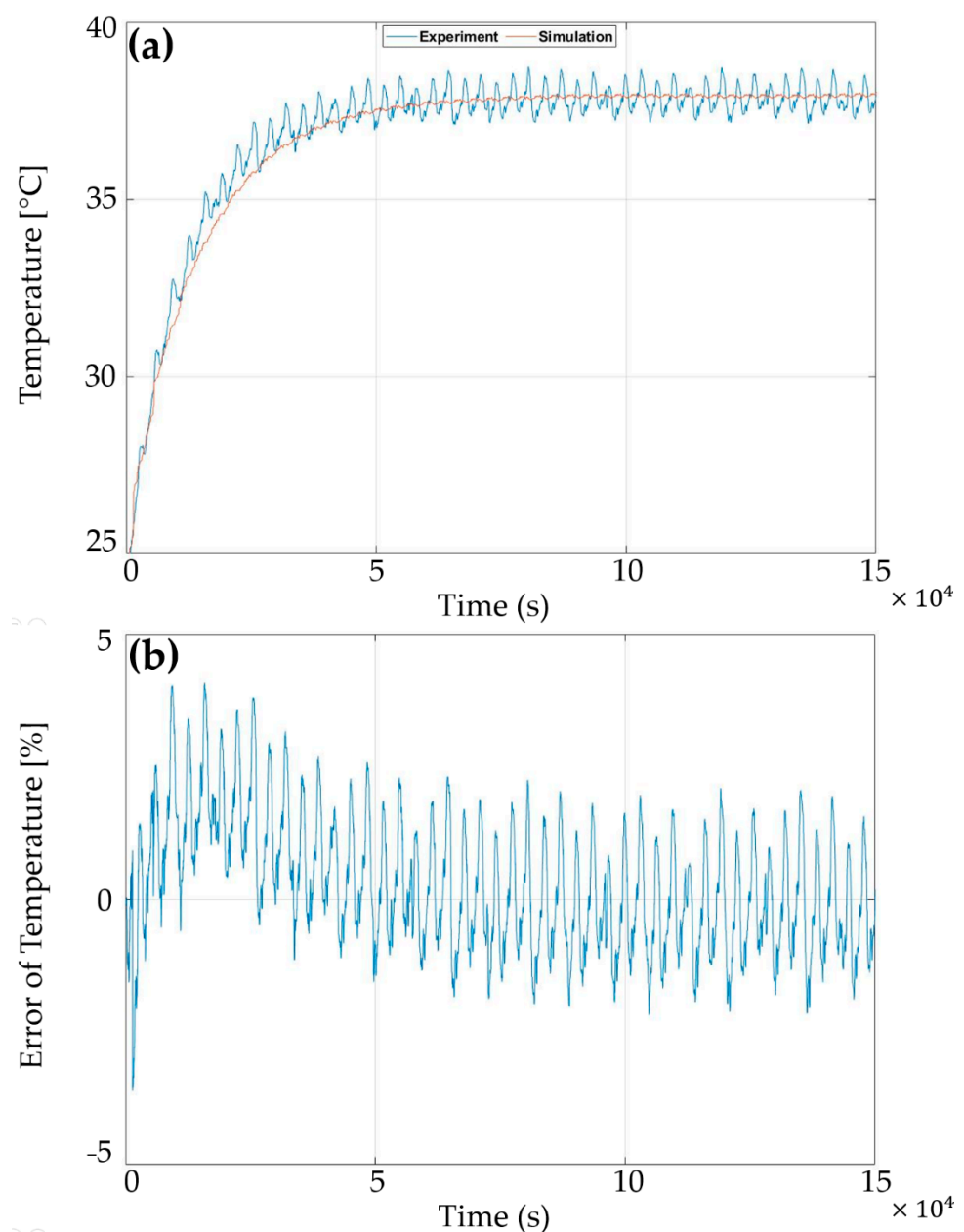


**Figure 14.** The developed 1D thermal model validation with the dynamic driving cycle for (a) experimental and simulation temperature; (b) error of temperature.

### 5.3. Results of the 3D CFD Model

The 3D CFD model is simulated by setting all the initial and boundary conditions for the system. The precision of the simulations is evaluated by validation of the results with experiments. With respect to this, all the case studies, including NC, pure PCM, and the hybrid PCM-HS, are modeled and validated against the experimental results. Figure 15 demonstrates the validation results of these use cases. As is evident, the CFD simulations for all the use cases perfectly match the experimental results, showing the precision of the extracted electrical and thermal parameters linked to the accurate 3D CFD model.

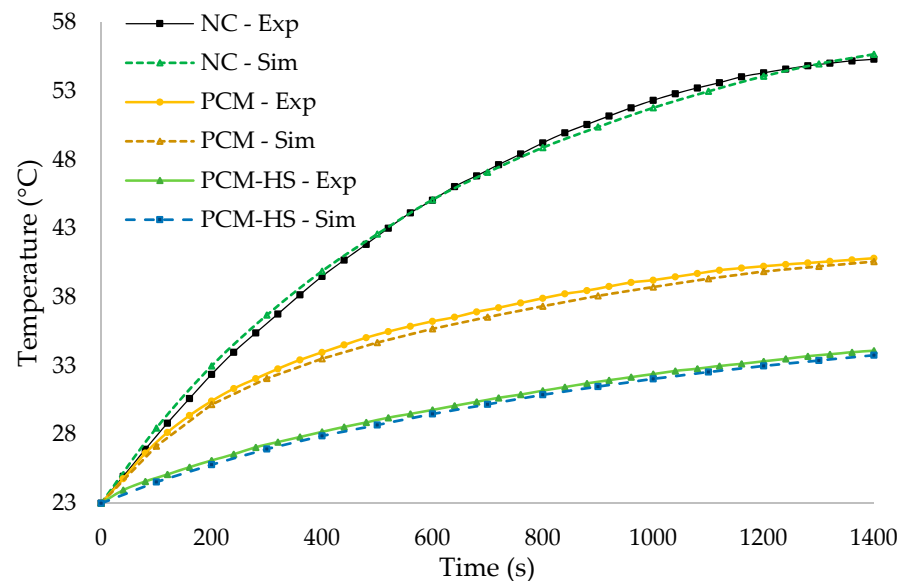


**Figure 15.** Validation of the 3D CFD analysis against the experimental results.

## 6. Conclusions

In this work, a prismatic 2300 F lithium-ion capacitor (LiC) was the target cell. The present paper aimed to develop a validated and robust coupled 1D–3D model capable of extracting the electrical and thermal parameters of the cell, which will then be used as an input to the 3D CFD model to investigate the thermal behavior of the LiC under the high dynamic current rate of 150 A. The 1D electro-thermal model was developed in a wide temperature range (from  $-30\text{ }^{\circ}\text{C}$  to  $+60\text{ }^{\circ}\text{C}$ ) under high current profiles (from 0.1 A to 500 A), which is unique. The electrical and thermal parameters were then extracted thanks to the robust 1D electro-thermal model and validated against the experiments. The extracted electrical parameters are open-circuit voltage (OCV), polarization capacitance and resistance, and internal series resistance. In addition, the power loss of the LiC was extracted using the 1D thermal model. Using the extracted electrical parameters, the electrical model was validated in such a high dynamic driving profile, in which the error for high current rates above 100 A was around  $\pm 5\%$ . For the currents lower than 100 A, the simulation error for voltage was lower than  $\pm 3\%$ , proving the precision of the developed electrical model. The temperature error in the thermal model in the worst scenario (the highest current rate) was around  $\pm 4\%$ . When the temperature of the LiC was at the steady-state zone, the error was below  $\pm 2\%$ , which is perfect for such a high dynamic profile.

Moreover, a 3D CFD model was linked to the 1D model to employ the extracted parameters and to be validated versus experimental tests. In this context, a test bench including PCM and heat sink (PCM-HS) was proposed to cool down the cell when working continuously under a high current rate of 150 A. Three different case studies were defined: natural convection (NC), pure PCM cooling system, and hybrid PCM-HS as the proposed hybrid TMS. The results exhibited that the temperature of the LiC under NC experiences very high temperatures above  $55\text{ }^{\circ}\text{C}$  that limit the cell's lifetime. When the PCM was used

as the TMS, the maximum temperature of the cell was controlled at 40.8 °C that shows a 26.2% improvement compared to the NC case study. Using the hybrid PCM-HS controlled the temperature of the cell around 34.1 °C, which shows a 38.3% enhancement compared to the NC. This proves the claim that, when a secondary passive system is added to the PCM to improve its thermal conductivity, the efficiency of such a passive system increases sharply, even at very high current rates.

The combined results of the 1D electro-thermal model and 3D thermal model show that the coupled model is very accurate for the high current rate of 150 A. The development of such a robust database will help to investigate the behavior of the LiC cell. Nevertheless, future work would be testing the proposed passive TMS for higher currents like 200 A, where the LiC will generate enormous heat.

**Author Contributions:** Conceptualization, methodology, software, validation, formal analysis, investigation, writing—original journal draft, D.K.; writing, review and editing, H.B. and M.A.; supervision, review and editing, J.V.M. and M.B. All authors have read and agreed to the published version of the manuscript.

**Funding:** This research received no external funding.

**Institutional Review Board Statement:** Not applicable.

**Informed Consent Statement:** Not applicable.

**Data Availability Statement:** Not applicable.

**Acknowledgments:** The authors acknowledge JSR Micro NV for their support for this research, and also Flanders Make for the support to our research group.

**Conflicts of Interest:** The authors declare no conflict of interest.

## References

1. Soltani, M.; Beheshti, S.H. A comprehensive review of lithium ion capacitor: Development, modelling, thermal management and applications. *J. Energy Storage* **2020**, *34*, 102019. [[CrossRef](#)]
2. Gandoman, F.H.; Behi, H.; Berecibar, M.; Jaguemont, J.; Aleem, S.H.A.; Behi, M.; Van Mierlo, J. Chapter 16—Reliability Evaluation of Li-ion Batteries for Electric Vehicles Applications from the Thermal Perspectives. In *Uncertainties in Modern Power Systems*; Zobia, A.F., Abdel Aleem, S.H.E., Eds.; Academic Press: Cambridge, MA, USA, 2021; pp. 563–587. [[CrossRef](#)]
3. Khaleghi, S.; Karimi, D.; Beheshti, S.H.; Hosen, M.S.; Behi, H.; Berecibar, M.; Van Mierlo, J. Online health diagnosis of lithium-ion batteries based on nonlinear autoregressive neural network. *Appl. Energy* **2021**, *282*, 116159. [[CrossRef](#)]
4. Soltani, M.; Ronsmans, J.; Kakihara, S.; Jaguemont, J.; Van den Bossche, P.; Van Mierlo, J.; Omar, N. Hybrid battery/lithium-ion capacitor energy storage system for a pure electric bus for an urban transportation application. *Appl. Sci.* **2018**, *8*, 1176. [[CrossRef](#)]
5. Jaguemont, J.; Karimi, D.; Van Mierlo, J. Investigation of a passive thermal management system for lithium-ion capacitors. *IEEE Trans. Veh. Technol.* **2019**, *68*, 10518–10524. [[CrossRef](#)]
6. Soltani, M.; Berckmans, G.; Jaguemont, J.; Ronsmans, J.; Kakihara, S.; Hegazy, O.; Van Mierlo, J.; Omar, N. Three dimensional thermal model development and validation for lithium-ion capacitor module including air-cooling system. *Appl. Therm. Eng.* **2019**, *153*, 264–274. [[CrossRef](#)]
7. Karimi, D.; Khaleghi, S.; Behi, H.; Beheshti, H.; Hosen, M.S.; Akbarzadeh, M.; Van Mierlo, J.; Berecibar, M. Lithium-ion capacitor lifetime extension through an optimal thermal management system for smart grid applications. *Energies* **2021**, *14*, 2907. [[CrossRef](#)]
8. Karimi, D.; Behi, H.; Jaguemont, J.; Berecibar, M.; Van Mierlo, J. A refrigerant-based thermal management system for a fast charging process for lithium-ion batteries. In *International Conference on Renewable Energy Systems and Environmental Engineering*; Global Publisher: Brussels, Belgium, 2020; pp. 1–6.
9. Hosen, M.S.; Karimi, D.; Kalogiannis, T.; Pirooz, A.; Jaguemont, J.; Berecibar, M.; Van Mierlo, J. Electro-aging model development of nickel-manganese-cobalt lithium-ion technology validated with light and heavy-duty real-life profiles. *J. Energy Storage* **2020**, *28*, 101265. [[CrossRef](#)]
10. Omar, N.; Daoud, M.; Hegazy, O.; Al Sakka, M.; Coosemans, T.; Van den Bossche, P.; Van Mierlo, J. Assessment of lithium-ion capacitor for using in battery electric vehicle and hybrid electric vehicle applications. *Electrochim. Acta* **2012**, *86*, 305–315. [[CrossRef](#)]
11. Firouz, Y.; Omar, N.; Timmermans, J.M.; Van Den Bossche, P.; Van Mierlo, J. Lithium-ion capacitor—Characterization and development of new electrical model. *Energy* **2015**, *83*, 597–613. [[CrossRef](#)]
12. Soltani, M.; De Sutter, L.; Ronsmans, J.; Van Mierlo, J. A high current electro-thermal model for lithium-ion capacitor technology in a wide temperature range. *J. Energy Storage* **2020**, *31*, 101624. [[CrossRef](#)]

13. Behi, H.; Behi, M.; Karimi, D.; Jaguemont, J.; Ghanbarpour, M.; Behnia, M.; Berecibar, M.; Van Mierlo, J. Heat pipe air-cooled thermal management system for lithium-ion batteries: High power applications. *Appl. Therm. Eng.* **2020**, *183*, 116240. [[CrossRef](#)]
14. Behi, H.; Karimi, D.; Jaguemont, J.; Gandoman, F.H.; Kalogiannis, T.; Berecibar, M.; Van Mierlo, J. Novel thermal management methods to improve the performance of the Li-ion batteries in high discharge current applications. *Energy* **2021**, *224*, 120165. [[CrossRef](#)]
15. Karimi, D.; Hosen, M.S.; Behi, H.; Khaleghi, S.; Akbarzadeh, M.; Van Mierlo, J.; Berecibar, M. A hybrid thermal management system for high power lithium-ion capacitors combining heat pipe with phase change materials. *Heliyon* **2021**, *7*, e07773. [[CrossRef](#)] [[PubMed](#)]
16. Karimi, D.; Behi, H.; Jaguemont, J.; Berecibar, M.; Van Mierlo, J. Optimized air-cooling thermal management system for high power lithium-ion capacitors. *Energy Perspect* **2020**, *1*, 93–105.
17. Möller, S.; Karimi, D.; Vanegas, O.; El Baghdadi, M.; Kospach, A.; Lis, A.; Hegazy, O.; Abart, C.; Offenbach, Â.B.Â. Application Considerations for Double Sided Cooled Modules in Automotive Environment. 2020. Available online: <https://ieeexplore.ieee.org/document/9097721> (accessed on 16 November 2020).
18. Akbarzadeh, M.; Jaguemont, J.; Kalogiannis, T.; Karimi, D.; He, J.; Jin, L.; Xie, P.; Van Mierlo, J.; Berecibar, M. A novel liquid cooling plate concept for thermal management of lithium-ion batteries in electric vehicles. *Energy Convers. Manag.* **2021**, *231*, 113862. [[CrossRef](#)]
19. Karimi, D.; Behi, H.; Hosen, M.S.; Jaguemont, J.; Berecibar, M.; Van Mierlo, J. A compact and optimized liquid-cooled thermal management system for high power lithium-ion capacitors. *Appl. Therm. Eng.* **2021**, *185*, 116449. [[CrossRef](#)]
20. Behi, H.; Karimi, D.; Behi, M.; Jaguemont, J.; Ghanbarpour, M.; Behnia, M.; Berecibar, M.; Van Mierlo, J. Thermal management analysis using heat pipe in the high current discharging of lithium-ion battery in electric vehicles. *J. Energy Storage* **2020**, *32*, 101893. [[CrossRef](#)]
21. Karimi, D.; Behi, H.; Jaguemont, J.; Berecibar, M.; Van Mierlo, J. Investigation of extruded heat sink assisted air cooling system for lithium-ion capacitor batteries. In *International Conference on Renewable Energy Systems and Environmental Engineering*; Global Publisher: Brussels, Belgium, 2020; pp. 1–6.
22. Karimi, D.; Jaguemont, J.; Behi, H.; Berecibar, M.; Van Den Bossche, P.; Van Mierlo, J. Passive cooling based battery thermal management using phase change materials for electric vehicles. In *EVS33 International Electric Vehicle Symposium*; The Electric Drive Transportation Association: Washington, DC, USA, 2020; pp. 1–12.
23. Behi, H. Experimental and Numerical Study on Heat Pipe Assisted PCM Storage System. 2015. Available online: <https://www.diva-portal.org/smash/get/diva2:850104/FULLTEXT01.pdf> (accessed on 13 September 2021).
24. Behi, H.; Karimi, D.; Behi, M.; Ghanbarpour, M.; Jaguemont, J.; Sokkeh, M.A.; Gandoman, F.H.; Berecibar, M.; Van Mierlo, J. A new concept of thermal management system in Li-ion battery using air cooling and heat pipe for electric vehicles. *Appl. Therm. Eng.* **2020**, *174*, 115280. [[CrossRef](#)]
25. Behi, H.; Karimi, D.; Jaguemont, J.; Gandoman, F.H.; Khaleghi, S.; Van Mierlo, J.; Berecibar, M. Aluminum heat sink assisted air-cooling thermal management system for high current applications in electric vehicles. In *Proceedings of the 2020 AEIT International Conference of Electrical and Electronic Technologies for Automotive, AEIT Automot*, Turin, Italy, 18–20 November 2020; Institute of Electrical and Electronics Engineers Inc.: Piscataway, NJ, USA, 2020. [[CrossRef](#)]
26. Behi, H.; Karimi, D.; Jaguemont, J.; Berecibar, M.; Van Mierlo, J. Experimental study on cooling performance of flat heat pipe for lithium-ion battery at various inclination angles. *Energy Perspect* **2020**, *1*, 77–92.
27. Behi, H.; Ghanbarpour, M.; Behi, M. Investigation of PCM-assisted heat pipe for electronic cooling. *Appl. Therm. Eng.* **2017**, *127*, 1132–1142. [[CrossRef](#)]
28. Behi, M.; Mirmohammadi, S.A.; Ghanbarpour, M.; Behi, H.; Palm, B. Evaluation of a novel solar driven sorption cooling/heating system integrated with PCM storage compartment. *Energy* **2018**, *164*, 449–464. [[CrossRef](#)]
29. Karimi, D.; Behi, H.; Jaguemont, J.; Sokkeh, M.A.; Kalogiannis, T.; Hosen, M.S.; Berecibar, M.; Van Mierlo, J. Thermal performance enhancement of phase change material using aluminum-mesh grid foil for lithium-capacitor modules. *J. Energy Storage* **2020**, *30*, 101508. [[CrossRef](#)]
30. Pu, L.; Zhang, S.; Xu, L.; Ma, Z.; Wang, X. Numerical study on the performance of shell-and-tube thermal energy storage using multiple PCMs and gradient copper foam. *Renew. Energy* **2021**, *174*, 573–589. [[CrossRef](#)]
31. Behi, M.; Shakorian-Poor, M.; Mirmohammadi, S.A.; Behi, H.; Rubio, J.I.; Nikkam, N.; Farzaneh-Gord, M.; Gan, Y.; Behnia, M. Experimental and numerical investigation on hydrothermal performance of nanofluids in micro-tubes. *Energy* **2020**, *193*, 116658. [[CrossRef](#)]
32. Behi, H.; Karimi, D.; Gandoman, F.H.; Akbarzadeh, M.; Khaleghi, S.; Kalogiannis, T.; Hosen, M.S.; Jaguemont, J.; Van Mierlo, J.; Berecibar, M. PCM assisted heat pipe cooling system for the thermal management of an LTO cell for high-current profiles. *Case Stud. Therm. Eng.* **2021**, *25*, 100920. [[CrossRef](#)]
33. Behi, H.; Karimi, D.; Youssef, R.; Suresh Patil, M.; Van Mierlo, J.; Berecibar, M. Comprehensive Passive Thermal Management Systems for Electric Vehicles. *Energies* **2021**, *14*, 3881. [[CrossRef](#)]
34. Karimi, D.; Behi, H.; Jaguemont, J.; El Baghdadi, M.; Van Mierlo, J.; Hegazy, O. Thermal Concept Design of MOSFET Power Modules in Inverter Subsystems for Electric Vehicles. In *Proceedings of the 2019 9th International Conference on Power and Energy Systems ICPES*, Perth, Australia, 10–12 December 2019. [[CrossRef](#)]

35. Kalbasi, R. Introducing a novel heat sink comprising PCM and air—Adapted to electronic device thermal management. *Int. J. Heat Mass Transf.* **2021**, *169*, 120914. [[CrossRef](#)]
36. Zhang, C.; Allafi, W.; Dinh, Q.; Ascencio, P.; Marco, J. Online estimation of battery equivalent circuit model parameters and state of charge using decoupled least squares technique. *Energy* **2018**, *142*, 678–688. [[CrossRef](#)]
37. Samba, A.; Omar, N.; Gualous, H.; Firouz, Y.; Van Den Bossche, P.; Van Mierlo, J.; Boubekeur, T.I. Development of an Advanced Two-Dimensional Thermal Model for Large size Lithium-ion Pouch Cells. *Electrochim. Acta* **2014**, *117*, 246–254. [[CrossRef](#)]
38. Firouz, Y.; Omar, N.; Van Den Bossche, P.; Van Mierlo, J. Electro-thermal modeling of new prismatic lithium-ion capacitors. In Proceedings of the 2014 IEEE Vehicle Power and Propulsion Conference (VPPC), Coimbra, Portugal, 27–30 October 2014; Volume 2, pp. 1–6. [[CrossRef](#)]
39. Sheikholeslami, M.; Ganji, D.D. Heat transfer enhancement in an air to water heat exchanger with discontinuous helical turbulators; experimental and numerical studies. *Energy* **2016**, *116*, 341–352. [[CrossRef](#)]
40. Panchal, S.; Dincer, I.; Agelin-Chaab, M.; Fraser, R.; Fowler, M. Experimental and theoretical investigations of heat generation rates for a water cooled LiFePO<sub>4</sub> battery. *Int. J. Heat Mass Transf.* **2016**, *101*, 1093–1102. [[CrossRef](#)]
41. Dutil, Y.; Rousse, D.R.; Salah, N.B.; Lassue, S.; Zalewski, L. A review on phase-change materials: Mathematical modeling and simulations. *Renew. Sustain. Energy Rev.* **2011**, *15*, 112–130. [[CrossRef](#)]
42. Farid, M.M.; Hamad, F.A.; Abu-Arabi, M. Melting and solidification in multi-dimensional geometry and presence of more than one interface. *Energy Convers. Manag.* **1998**, *39*, 809–818. [[CrossRef](#)]
43. National Renewable Energy Laboratory (NREL). Battery Lifetime Analysis and Simulation Tool Suite 2014. Available online: <https://www.nrel.gov/docs/fy15osti/63246.pdf> (accessed on 1 December 2014).